Loss of the apical V-ATPase a-subunit VHA-6 prevents acidification of the intestinal lumen during a rhythmic behavior in C. elegans

Erik Allman, David Johnson and Keith Nehrke

Am J Physiol Cell Physiol 297:1071-1081, 2009. First published Sep 9, 2009;
doi:10.1152/ajpcell.00284.2009

Am J Physiol Cell Physiol 297: C1071–C1081, 2009.
First published September 9, 2009; doi:10.1152/ajpcell.00284.2009.

Loss of the apical V-ATPase a-subunit VHA-6 prevents acidification of the intestinal lumen during a rhythmic behavior in *C. elegans*

Erik Allman,[1] David Johnson,[2] and Keith Nehrke[1,3]

Departments of [1]Pharmacology and Physiology, [2]Biochemistry, and [3]Medicine, University of Rochester Medical Center, Rochester, New York

Submitted 1 July 2009; accepted in final form 9 September 2009

Allman E, Johnson D, Nehrke K. Loss of the apical V-ATPase a-subunit VHA-6 prevents acidification of the intestinal lumen during a rhythmic behavior in *C. elegans*. *Am J Physiol Cell Physiol* 297: C1071–C1081, 2009. First published September 9, 2009; doi:10.1152/ajpcell.00284.2009.—In *Caenorhabditis elegans*, oscillations of intestinal pH contribute to the rhythmic defecation behavior, but the acid-base transport mechanisms that facilitate proton movement are not well understood. Here, we demonstrate that VHA-6, an intestine-specific a-subunit of the H^+-K^+-ATPase complex (V-ATPase), resides in the apical membrane of the intestinal epithelial cells and is required for luminal acidification. Disruption of the *vha-6* gene led to early developmental arrest; the arrest phenotype could be complemented by expression of a fluorescently labeled *vha-6* transgene. To study the contribution of *vha-6* to pH homeostasis in larval worms, we used a partial reduction of function through postembryonic single-generation RNA interference. We demonstrate that the inability to fully acidify the intestinal lumen coincides with a defect in pH recovery of the intestinal epithelial cells, suggesting that VHA-6 is essential for proton pumping following defecation. Moreover, intestinal dipeptide accumulation and fat storage are compromised by the loss of VHA-6, suggesting that luminal acidification promotes nutrient uptake in worms, as well as in mammals. Since acidified intracellular vesicles and autofluorescent storage granules are indistinguishable between the *vha-6* mutant and controls, it is likely that the nutrient-restricted phenotype is due to a loss of plasma membrane V-ATPase activity specifically. These data establish a simple genetic model for proton pump-driven acidification. Since defecation occurs at 45-s intervals in worms, this model represents an opportunity to study acute regulation of V-ATPase activity on a short time scale and may be useful in the study of alternative treatments for acid-peptic disorders.

biorhythm; nematode; proton

RHYTHMIC BEHAVIORS occur among nearly all organisms, with periods ranging from seconds to days to years. The soil nematode *Caenorhabditis elegans* exhibits an ultradian defecation cycle with a 45- to 50-s period that is tightly regulated in well-fed animals (12, 64) but, similar to many rhythmic behaviors, is subject to modulation by environmental factors (27, 57). Because the defecation motor program (DMP) is readily observable, it has formed the basis for a number of genetic screens (27, 40, 64). The results of these screens have led to a preliminary understanding of the basal molecular components involved in defecation signaling.

The DMP is initiated through the rhythmic generation of inositol 1,4,5-trisphosphate-dependent calcium signals in the intestine (15, 16, 45, 50, 62). Oscillatory calcium signaling triggers the contraction of posterior body wall muscles (pBoc) through the secretion of protons by the sodium-proton exchanger PBO-4/NHX-7 across the basolateral surface of the intestine (3, 51). In addition, proton equivalents move from the lumen (pH ~4.1) to the cytoplasm (pH ~7.4) during defecation, resulting in rhythmic pH oscillations that mimic calcium oscillations in frequency; this may be an effort to conserve protons, which would otherwise be lost during expulsion of the luminal contents following defecation (51). Because the resting pH of the lumen is acidic relative to the cytoplasm, it is likely that establishment of the pH gradient across the apical membrane requires energy, and maintenance of an acidified lumen may be important for normal growth and/or viability. Thus the rhythmic defecation behavior in the nematode *C. elegans* represents a unique opportunity to study acid-base transport and its intersection with oscillatory calcium signaling and metabolism in a genetic model organism.

V-ATPases are large composite enzymes consisting of peripheral (V_1) and integral (V_0) membrane domains. Similar to F_0F_1-ATPases, they function to pump protons across cell membranes in exchange for the hydrolysis of ATP (8, 19, 25). V-ATPases are often found in the membranes of endosomes, lysosomes, and secretory vesicles, where they participate in acidification of the organelle and potentiate many of its functions (4). However, V-ATPases are also found at the plasma membrane, where they are involved in active proton transport and extracellular pH regulation, and defects in proton pumping form the molecular basis for a number of human diseases. For example, osteopetrosis occurs through a lack of bone resorption and has been shown to result from genetic lesions in carbonic anhydrase II (58, 70), the chloride channel ClC-7 (36), or the a_3-subunit of V-ATPase (37), which function together in osteoclasts to acidify the cleft between the resorptive cell and bone mineral (5, 28, 46, 72). Similarly, renal tubular acidosis results from a failure of the kidney to regulate systemic pH and can be caused by mutations in V-ATPase subunits (1, 10, 11, 30). Particularly relevant to this work is the finding that V-ATPase activity in parietal cells allows secretion of HCl into the stomach (18). As such, acid suppression, which is the major medical strategy for treatment of acid-peptic disorders, occurs through the use of proton pump inhibitors (PPIs) such as omeprazole. However, adverse effects of long-term use of PPIs may include hypergastrinemia, rebound acid hypersecretion, malabsorption, infection, and drug interactions (56). Although controversial in terms of its translation to humans (38), treatment with omeprazole eventually leads to carcinoid tumors in rats through gastrin stimulation of endochromaffin-like cells (23).

The *C. elegans* genome contains the coding potential for multiple V-ATPase subunit orthologs, including 19 *vha* genes, *unc-32*, and *spe-5*. These genes code for subunits A–H of the

Address for reprint requests and other correspondence: K. Nehrke, Nephrology Division, Dept. of Medicine, Medical Center Box 675, 601 Elmwood Ave., Rochester, NY 14642 (e-mail: keith_nehrke@urmc.rochester.edu).

V_1 rotor domain and subunits a, d, c, and c′′ and accessory subunits e and S1 of the V_0 proton-translocating domain; different genes code for several subunits, most notably, subunits a and c in worms. V-ATPases have been associated with multiple physiological functions in worms, including ovulation and embryogenesis (48), synaptic vesicle release from cholinergic neurons (52), apical trafficking/secretion of exosomes containing hedgehog-related proteins (39), necrotic cell death (61), formation of lysosomal fat storage granules in the intestine (24), and prevention of cell-cell fusion (35). In all these processes except cell fusion, the V-ATPase complexes are thought to function at the level of intracellular organelles, rather than at the plasma membrane, and it is unclear whether the antifusogenic role of V-ATPase requires proton transport.

Oka et al. (49) identified *vha-6* as one of four genes (*vha-5, vha-6, vha-7*, and *unc-32*) coding for the proton-translocating a-subunit in *C. elegans*. Mammals also express four a-subunit isoforms that are thought to be differentially targeted to specific cell membranes (67, 68), and mutation of these genes specifically has been associated with distal renal tubular acidosis and osteopetrosis. In worms, *vha-6* is strongly and exclusively expressed in the intestine, where RNA interference (RNAi) suggests that it is essential for larval development (49).

In the present study, we show that the VHA-6 protein is localized to the apical membrane and that its loss prevents full acidification of the intestinal lumen, which normally resides at pH ~4. Moreover, defective VHA-6 activity represses intracellular pH (pH_i) recovery following defecation, consistent with a role in proton pumping. Elimination of VHA-6 activity also appears to cause a defect in dipeptide uptake, leading to larval arrest through starvation and suggesting that the apical membrane proton gradient facilitates nutrient absorption processes in worms. These observations lead us to believe that functional aspects of the worm intestinal V-ATPase are conserved with acid secretion in the mammalian stomach and that studies in worms could lead to the identification of alternate therapeutic targets or strategies for acid suppression. Finally, the involvement of a V-ATPase in defecation affords an opportunity to exploit this rhythmic model behavior toward an understanding of acute regulation of proton pumps (6, 54).

MATERIALS AND METHODS

Strains, alleles, vectors, and culturing techniques. Standard genetic and culturing techniques were used (7). Nematodes were maintained at 20°C on normal growth medium (NGM)-agar plates buffered at pH ~6. For imaging studies, agarose was substituted for agar to reduce background fluorescence. The high-pH plates were made by alteration of the ratio of mono- to dibasic sodium phosphate in the buffer. The pH of the plates was confirmed by fluorescence imaging, which was carried out using a small amount of the pH probe BCECF-dextran placed on the surface of the plates. The wild-type strain is Bristol N2. The *vha-6(ok1825)* mutant was created by the *C. elegans* Gene Knockout Consortium and provided by the *C. elegans* Genetic Center. The mutant was outcrossed three times against N2 and balanced using mIn1 to create the strain KWN116 *vha-6(ok1825)*/mIn1[mIs14 *dpy-10(e128)*]II. The reporters have been described elsewhere (45, 51) and include the pH-sensitive green fluorescence protein (GFP) variant pHluorin, expressed exclusively in the intestinal cells and used to measure pH_i (P*nhx-2*::pHluorin); pHluorin fused as a chimera to the targeting domain(s) of PAT-3 and expressed at the basolateral membrane of posterior intestinal cells to measure extracellular pH (P*nhx-7*::PAT-3::pHluorin); and the calcium indicator YC6.12 expressed in the intestinal cells (P*nhx-2*::YC6.12). The constructs pELA1 (P*vha-6*::mCherry) and pELA2 (P*vha-6*::VHA-6::mCherry) were created by PCR amplification of N2 genomic DNA and cloning of the resulting fragments into the worm mCherry expression vector pCH1 using restriction sites tagged to the primers. The forward primer for both reactions was ACA GCT AGC AGC ACA GAA CTG CAT TAA GTA TAC, with the complementary portion underlined and the remainder consisting of an *Nhe* I restriction site tag. The reverse primers were ACA ACG TCG ACC CTC CGA TCT ATA GAT CGA GCC (with the complementary portion underlined and the remainder consisting of an *Sal* I restriction site tag) and ACA ACG TCG ACC CTG ATC GAG TCC CTC GTA AAC GC (with the complementary portion underlined and the remainder consisting of an *Sal* I restriction site tag) for the transcriptional promoter fusion pELA1 and the translational rescue fusion pELA2, respectively. The strains are KWN1 *pha-1(e2123ts)*III, *him-5(e1490)*V, and rnyEx001[P*nhx-2*::YC6.1, *pha-1*(+)]; KWN26 *pha-1(e2123ts)*III and rnyEx006[P*nhx-2*::pHluorin, *pha1*(+)]; KWN30 *pha-1(e2123ts)*III and rnyEx009[P*nhx-7*::PAT-3::pHluorin, *pha-1*(+)]; KWN112 *pha-1(e2123ts)*III, *him-5(e1490)*V, and rnyEx058[pELA1, *pha-1*(+)]; KWN117 *pha-1(e2123ts)*III, *him-5(e1490)*V, and rnyEx060 [pELA2; P*myo-3*::pHluorin; *pha-1*(+)]; and KWN118 *vha-6(ok1825)*II and rnyEx060.

RNAi. The vector used to target *vha-6* was obtained from a library created by Kamath et al. (29). Freshly transformed HT115 bacteria were grown at 37°C to mid-log phase, induced with 1 mM isopropylthiogalactopyranoside for 1 h, and seeded onto NGM plates. Stage L1 larval worms were placed onto the RNAi plates and allowed to mature at 20°C for 3 days before analysis. The control RNAi vector pPD129.36 (courtesy of A. Fire, Stanford University) does not contain an insert.

LysoTracker Red, AMCA-dipeptide, and Oil Red O staining. For LysoTracker Red (Molecular Probes, Eugene, OR) staining, 3-day post-L1 worms were incubated as described previously (24) on seeded plates containing dye (2 μM) for 12 h in the absence of light. For 7-amino-4-methylcoumarin-3-acetic acid (AMCA)-dipeptide loading, the worms were washed from their agar plates with S-Basal medium, pelleted by brief centrifugation, and then resuspended in 100 μl of S-Basal medium that contained 10% (vol/vol) feeder bacteria as well as 1 mM Ala-Lys-AMCA (courtesy of Dr. Hannelore Daniel) for 12 h at 20°C with vigorous shaking. After they were stained, all the worms were washed twice with S-Basal buffer and transferred to a 2% agarose pad in S-Basal medium with 0.1% ethyl 3-aminobenzoate (Tricaine) and 0.01% tetramisole for imaging. For staining with Oil Red O, worms were washed from their agar plates with S-Basal medium and pelleted by brief centrifugation. The supernatant was aspirated, and the worm pellets were resuspended in a buffer containing 150 mM KCl, 40 mM NaCl, 14 mM EGTA, 1 mM spermidine HCl, 0.4 mM spermine, 30 mM Na-PIPES (pH 7.4), 0.2% β-mercaptoethanol, and 1% paraformaldehyde. The worms were incubated on ice for 15 min and then permeabilized by three sequential freeze-thaw cycles in liquid nitrogen and a 50°C water bath. After permeabilization, the worms were spun down and resuspended in 60% isopropanol and then incubated in 60% saturated Oil Red O in 60% isopropanol. After 15 min, excess Oil Red O was washed away, and the worms were rehydrated in PBS and mounted onto slides.

Microscopy. Primarily, analysis was performed as described previously (51). The wavelengths for excitation (λ_{ex}) and emission (λ_{em}) of the various dyes are as follows: 340 nm λ_{ex} and 450 nm λ_{em} for AMCA, 555 nm λ_{ex} and 590 nm λ_{em} for LysoTracker Red, 435 nm λ_{ex} and 480/535 nm λ_{em} for YC6.12, 410/470 nm λ_{ex} and 535 nm λ_{em} for pHluorin, 555 nm λ_{ex} and 590 nm λ_{em} for mCherry, 490/440 nm λ_{ex} and 535 nm λ_{em} for Oregon Green or BCECF, and 340 nm λ_{ex} and 535 nm λ_{em} 535 for autofluorescence. Brightfield images were used for Oil Red O. Plan Apo objectives, including ×10 and ×20 dry and ×40 and ×100 oil immersion, were used.

For measurements of ion flux, live-behaving worms were imaged on NGM-agarose plates using a ×10 Plan Apo objective. To com-

pensate for the lack of physical restraints, we used a stage controller to keep the worms in the center of the field of view during the imaging process. A Nikon Eclipse TE2000-U inverted fluorescence microscope was equipped with an excitation monochromator (Polychrome IV, TILL Photonics) and a high-speed monochromatic camera (SensiCam, Cooke). Image capture and quantitative measurements were run through the TILLvisION software package (TILL Photonics), and execution of the DMP was denoted post hoc. For cytosolic (pH_i) and basolateral pH measurements, transgenic lines expressing the pH indicator protein pHluorin (43) were used. For conversion of the derivative fluorescent ratio to pH_i, the worm was gently sliced open with a 32-gauge needle immediately posterior to the pharyngeal-intestinal valve to expose the intestinal cells, and in situ calibration was performed using the high-K^+-nigericin technique (63). For luminal pH measurements, worms were washed from their NGM plates and pelleted by brief centrifugation. The worms were resuspended with bacterial food in a final volume of 50 μl, and an additional 50 μl of S-Basal buffer containing 5 mg/ml of an Oregon Green-dextran conjugate (70 kDa, Molecular Probes) were added. The worms were loaded with the conjugate by feeding for 2 h at 20°C on a rocking platform. The loaded worms were washed twice in S-Basal buffer containing 1 mg/ml BSA and returned to NGM-agarose plates for imaging. The fluorescence excitation ratio was converted to pH using an in vitro calibration curve for the dye in solution. For calcium measurements, images of the pH-insensitive yellow cameleon YC6.12 (69) were acquired at 2 Hz using an optical beamsplitter (Optical Insights, Tucson, AZ) coupled to the above-described rig.

Images of transgenic mCherry- and Oil Red O-stained worms were acquired at the University of Rochester Confocal Core using a FV1000 Olympus laser scanning confocal microscope with a ×20 objective and an Olympus VanoxAH-2 conventional microscope with a ×10 objective, respectively. Staining intensities were quantified using TILLvisION software.

RESULTS

Intestinal V-ATPase a-subunit VHA-6 is required for larval growth. VHA-6 is an a-subunit that forms part of the vacuolar-type K^+-H^+-ATPase (V-ATPase) V_0 domain. The V_0 domain is membrane associated and is responsible for proton translocation. Previous work showed that VHA-6 is expressed specifically in the 20 epithelial cells of the intestine and is targeted to the apical plasma membrane, rather than an organelle (49). We confirmed this result by creating fusions of the *vha-6* promoter and genomic coding region to the red-fluorescent protein mCherry in transgenic worms, as shown schematically in Fig. 1*A*. The promoter::mCherry fusion was expressed in the intestine of larval and adult worms (Fig. 1*B*), whereas a COOH-terminal translational fusion of VHA-6 to mCherry was targeted to the apical membrane (Fig. 1*C*), as demonstrated clearly by cross-sectional images in the *y*- and *z*-planes extracted from a confocal stack (Fig. 1*D*).

To assess the function of VHA-6 in intestinal physiology, we obtained a strain containing a deletion in the *vha-6* gene, which was created by the *C. elegans* Gene Knockout Consortium. The *vha-6(ok1825)* allele is a 982-bp excision that results in the loss of 297 amino acids of coding region near the center of the gene and is predicted to result in a nonfunctional protein. We found that *vha-6* is essential, inasmuch as development of extensively outcrossed *ok1825* homozygotes was arrested soon after the worms hatched (Fig. 2). To confirm that the loss of VHA-6 was responsible for the larval arrest phenotype, a P*vha-6*::VHA-6::mCherry transgene such as that shown in Fig. 1 was expressed from an extrachromosomal array in transgenic worms. The red-fluorescent-tagged VHA-6 protein completely rescued developmental arrest and resulted in worms that were nearly indistinguishable from wild-type worms (Fig. 2, *C* and *D*).

Mosaicism refers to the process by which extrachromosomal arrays are lost during cell division. For confirmation that the array was required for rescue, 50 mosaic animals completely lacking fluorescence were chosen from the *vha-6* mutant line and moved to a fresh plate. These worms reverted to the mutant phenotype and never progressed beyond the L1 stage (Fig. 2, *A* and *B*).

The arrested development of the *vha-6(ok1825)* homozygotes and, thus, their failure to exhibit normal rhythmic physiological processes complicated study of the role of VHA-6 in postembryonic intestinal physiology and pH balance during defecation. However, even genes whose genomic loss leads to death can be studied using double-stranded RNA-mediated

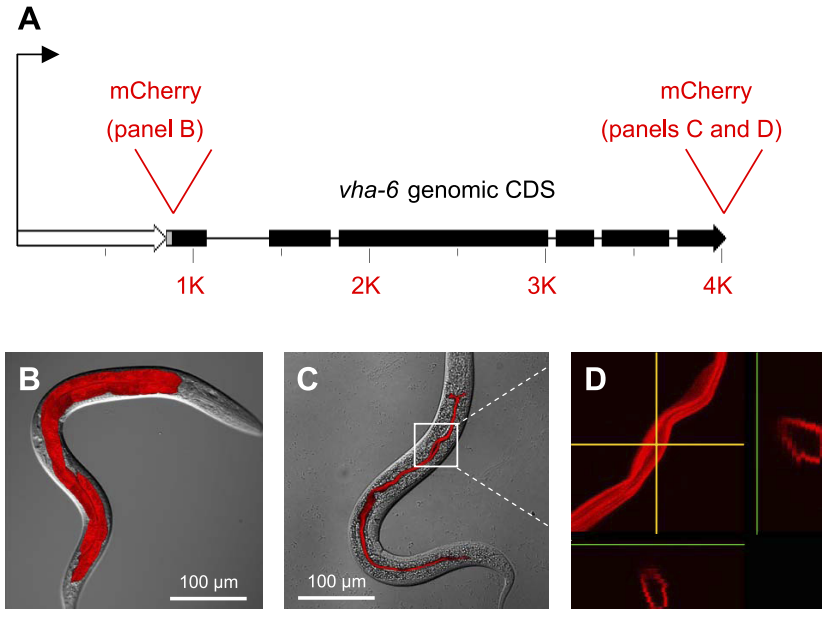

Fig. 1. Expression and localization of the *vha-6* gene product in transgenic worms. *A*: *vha-6* promoter (open arrow) and genomic coding region (filled arrow) and sites where mCherry cDNA was inserted to create transcriptional and translational fusions are depicted to scale. *B*: transcriptional fusion to the 1,023-nucleotide promoter results in mCherry expression restricted exclusively to intestinal epithelia of the worm at the L4 stage. *C*: translational fusion that included the promoter and the genomic coding region fused in-frame to the mCherry cDNA results in protein targeting to the apical membrane of intestinal epithelial cells of the L4 hermaphrodite. *B* and *C* are overlays of confocal microscopy maximum projection images onto their corresponding differential interference contrast (DIC) images. *D*: magnification of the portion of *C* enclosed in the white box and display of cross-sectional images in *y*- and *z*-planes (yellow arrows) clearly demonstrate that the fusion protein lies at or near the apical surface. CDS, coding region.

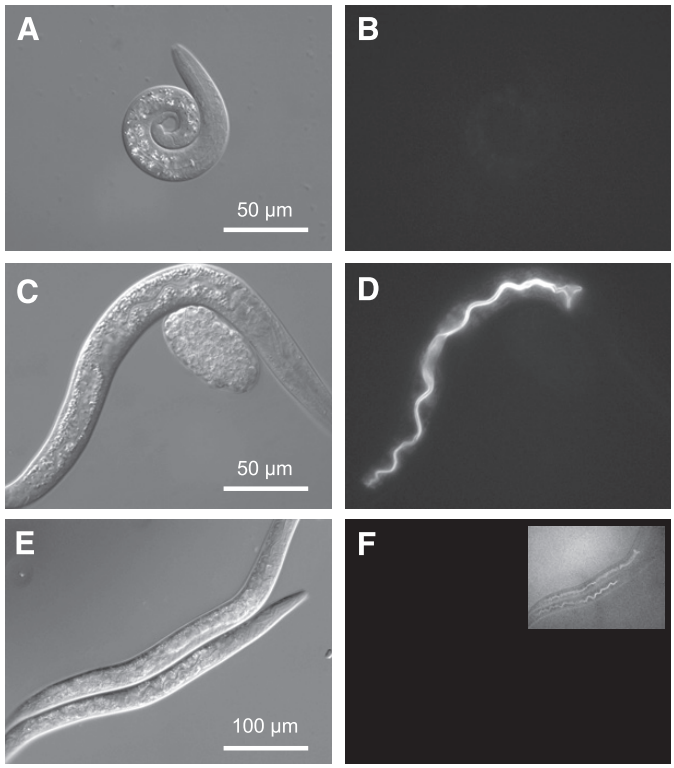

Fig. 2. Analysis of *vha-6* mutant and RNA interference (RNAi) phenotypes. *A, C*, and *E* are DIC contrast images; *B, D*, and *F* are fluorescent images. Homozygous *vha-6(ok1825)* deletion mutants (courtesy of the *C. elegans* Gene Knockout Consortium) arrested development as L1 larva, but an extrachromosomal array coding for a P*vha-6*::VHA-6::mCherry translational fusion could complement the mutation and restore normal growth. To illustrate this, we examined brethren from the rescued line where mosaic loss of the rescue construct at 15°C resulted in worms that lacked fluorescence and arrested development as L1 larvae (*A* and *B*; 48-h posthatch L1 arrest), whereas the presence of the construct in age-matched transgenic siblings restored normal development (*C* and *D*; 48-h posthatch L2/L3). Single-generation treatment of wild-type worms with *vha-6* RNAi for 3 days, starting as a recently hatched L1 larva, reduced VHA-6::mCherry expression to nearly undetectable levels (*F*; *inset* is 10-fold longer exposure). RNAi-treated worms exhibited a progressive slowing of growth, such that they had generally reached the L3/L4 stage by 72 h and often never reached reproductive maturity (*E*). These phenotypes are consistent with a requirement for VHA-6 activity for growth and maturation.

gene interference (RNAi) in worms (13). For our studies, single-generation RNAi was performed by exposure of recently hatched L1 larva to double-stranded RNA that targets *vha-6*. This approach allowed us to study the progressive effects of loss of VHA-6 over time. To confirm the effectiveness of this treatment, worms expressing the mCherry-labeled rescue transgene were treated with RNAi. At 3 days after exposure, levels of intestinal VHA-6::mCherry expression were greatly reduced (<5%) compared with the *vha-6(RNAi)* worms, although faint residual expression was noted, consistent with the incomplete effectiveness of RNAi (Fig. 2, *E* and *F*). Phenotypically, the *vha-6(RNAi)* worms exhibited a variably reduced growth rate, and at 72 h the population consisted mainly of L3–L4 larva, with a small number of extremely small adults, whereas control worms had entered reproductive adulthood (data not shown). Of the *vha-6(RNAi)* worms that did enter adulthood, their progeny exhibited L1 arrest, consistent with the phenotype of the deletion mutant.

The single-generation *vha-6(RNAi)* worms continued to defecate at 72 h; however, we noted that defecation ceased at later time points (i.e., 5 days and beyond). To control for this, our experiments were generally performed with worms that had been on RNAi plates for 3 days at 20°C starting as L1 larva, and their ability to defecate was assessed before further analysis. This model likely represents a significant, but not complete, reduction of VHA-6 activity and was necessary for study of the physiological role of VHA-6 in the rhythmic defecation behavior. The data in Table 1 indicate that, at 72 h after exposure, the RNAi-mediated loss of *vha-6* expression extended the defecation cycle period [58.6 ± 2.5 s (n = 17) vs. 44.6 ± 1.5 s (n = 9) for control worms] and caused a slight arrhythmia [coefficient of variation = 12.9 ± 6.1% (n = 17) vs. 5.3 ± 2.9% (n = 9) for control worms].

VHA-6 contributes to pumping protons from the intestinal cytoplasm into the lumen following defecation. On average, a wild-type worm defecates at ~45-s intervals (64). The defecation period is controlled by intestinal oscillatory calcium signaling (15, 16), which triggers pH fluctuations inside and outside the cell (3, 51). Here, we used a combination of fluorescent biosensors, pH-sensitive dyes, and RNAi to assess the contribution of VHA-6 to pH homeostasis during the defecation cycle. Our measurements were performed using real-time fluorescence imaging in unrestrained worms in the presence of ample food, so as not to influence the behavioral readout, as described previously (45, 51). Representative pH traces from single worms are presented in Fig. 3*A* for clarity (for averaged traces from multiple worms followed over numerous cycles, see supplemental Fig. S1 in the online version of this article); detailed statistical analyses are shown in Table 1.

Measurements of pH_i utilized transgenic expression of the biosensor pHluorin (43) in the intestinal epithelia. In control worms, pH_i oscillated once per defecation cycle, and acidification clearly presaged the execution of pBoc (Fig. 3*A*). The average resting pH (n = 4) was 7.52 ± 0.04; a slow acidification over 10–15 s of ~0.09 unit was followed by a rapid decline to 7.11 ± 0.02 (Table 1, also see supplemental Fig. S1A). In *vha-6(RNAi)* worms, pH oscillated once per cycle as well (Fig. 3*A*), but the oscillations were diminished in amplitude (Table 1, also see supplemental Fig. S1B; ΔpH = 0.16 ± 0.02 vs. 0.32 ± 0.05 in controls), and the cells were relatively acidic (resting pH = 7.29 ± 0.03 vs. 7.52 ± 0.04 in controls). Although the amplitude of the oscillations was diminished, the

Table 1. *Characteristics of pBoc and intestinal pH oscillations in control and vha-6(RNAi) worms*

	pBoc Period, s	pBoc CV, %	pBoc Contraction, %	ΔpH_i	ΔpH_{lumen}
Control	44.6±1.5 (9)	5.3±2.9 (9)	13.7±3.0 (6)	0.32±0.05 (4)	1.93±0.17 (7)
Vha-6(RNAi)	58.6±2.5* (17)	12.9±6.1* (17)	16.9±1.6 (8)	0.16±0.02* (4)	0.34±0.21* (4)

Values are means ± SD of number of worms in parentheses. Fluorescent images were acquired at 0.5-s intervals. pBOC, posterior body wall muscles; pH_i, cytoplasmic pH; CV, coefficient of variation. *$P < 0.01$ vs. control.

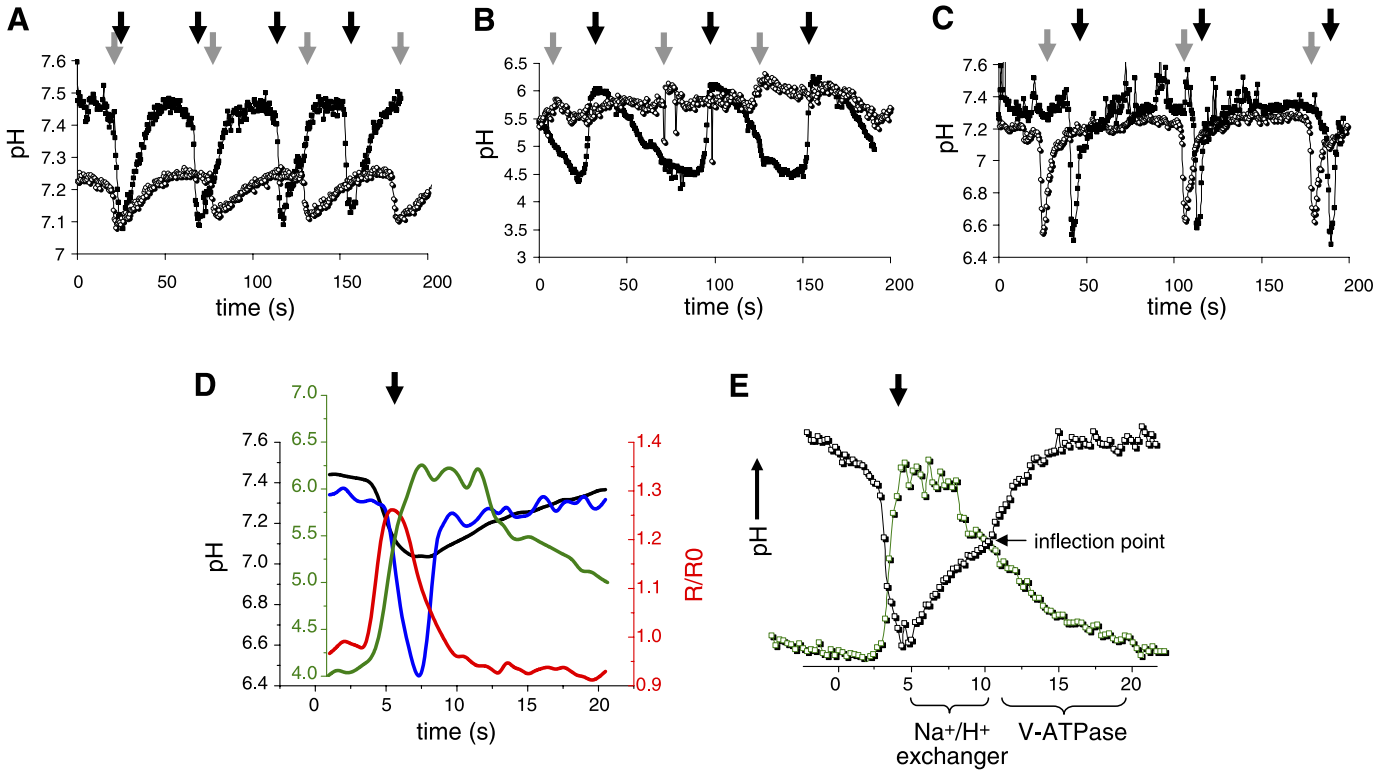

Fig. 3. Analysis of intestinal pH dynamics in free-range worms. Representative traces from single 72-h posthatch animals show intracellular pH oscillations (*A*), luminal pH oscillations (*B*), and basolateral, extracellular pH oscillations (*C*) in control (■) and *vha-6(RNAi)* (○) worms imaged over 200 s while moving freely on bacteria-seeded plates. pBoc is signified by dark arrows (control) and gray arrows (*vha-6*) to show time intervals for a complete defecation period in the worms. Intracellular and luminal data (*A* and *B*) were collected from worms in which RNAi feeding was initiated upon hatching. Because the extracellular pH biosensor is not expressed well in larva, to allow development to adulthood, we collected basolateral data (*C*) from worms exposed to RNAi at the L3 stage. Their older age likely accounts for their somewhat extended defecation period. Average traces of single cycles from multiple worms are shown in the supplemental data, and statistics are provided in Table 1. *D*: representation of intestinal pH [intracellular pH (pHi, black trace), luminal pH (green trace), and basolateral, extracellular pH (blue trace)] and calcium oscillations (red trace) during defecation. All traces are plotted to the axis of the same color, except the basolateral trace, which is plotted to the black axis, the same as pH_i. Individual traces have been normalized to the execution of pBoc at the start of defecation but were collected from separate worms and are not intended to depict exact temporal or causal relationships. R/R_0, ratio normalized to *time 0*. *E*: biphasic kinetics of pH_i recovery suggest that 2 ion transport processes function in sequence (black trace). The first phase is predicted to occur through Na^+/H^+ exchange, as indicated, which facilitates recovery from acidification in most cell types. This phase exhibits pH dependence and an apparent plateau near the inflection point. Whether these protons are exported from the cell across the basolateral or the apical membrane is unknown, although luminal pH is relatively stable during this first phase of cytoplasmic recovery (green trace). The second phase is clearly noted after the inflection point in the pH_i trace. During this phase, luminal pH begins to decrease as a result of proton pumping at the apical membrane, and the cell is driven to become more alkaline. Traces were not extracted from a single animal, and the relationship between cytoplasmic and luminal pH is intended to be representative, rather than absolute. Scale has been optimized for comparison (for actual values see Table 1)

relatively acidic resting pH_i resulted in a nadir pH that was statistically indistinguishable from controls (7.11 ± 0.02 vs. 7.13 ± 0.03).

Measurements of luminal pH utilized the pH-sensitive dye Oregon Green-dextran. This dye accumulates in the intestinal lumen when fed to worms, but it is rapidly expulsed during defecation. Nonetheless, several cycles of pH oscillations can be measured before the signal diminishes below the threshold for detection. In control worms, the luminal pH oscillated once per cycle, and a rapid alkalinization occurred coincident with pBoc (Fig. 3*B*). The average resting pH of the lumen (n = 4) was 4.35 ± 0.17; a rapid increase to 6.28 ± 0.16 was followed by a plateau phase near pH 6 and a slow reacidification over the following 30 s before the next cycle (Table 1, also see supplemental Fig. S1C). Worms treated with *vha-6* RNAi, on the other hand, exhibited strikingly reduced luminal pH oscillations that were nearly undetectable against background noise (Fig. 3*B*), with an average resting luminal pH (n = 4) of 5.49 ± 0.18 and an increase to 5.83 ± 0.24 during defecation (Table 1, also see supplemental Fig. S1D).

Figure 3*D* is a representation of intestinal calcium and pH oscillations during defecation. The relationships shown in Fig. 3*D* are schematized and are not intended to define absolute values, nor are they intended to show precise relative timing of electrolyte flux, particularly given that we cannot measure these parameters simultaneously. Instead, they are meant to illustrate the general relationships between each parameter measured in this work. However, recovery from intracellular acidification occurs in two stages, which are separated by an obvious inflection point (Fig. 3*E*); because our measurements are made in moving worms, sometimes slight movement artifacts can obscure this inflection point, but invariably there are two phases to the recovery process. A general comparison with the kinetics of luminal pH oscillations leads to several predictions. The first stage of intestinal pH recovery appears to begin at least without appreciable acidification of the intestinal lumen

(Fig. 3*E*), which could be due to buffering capacity of the lumen or initial efflux of protons predominantly through the basolateral membrane. We suggest that, during this period, sodium/proton exchangers may be facilitating pH recovery, akin to their role in mammalian cells, accounting for the pH dependence of recovery rate and the seeming plateau that would be reached were the second stage of recovery not triggered. This second stage drives the resting pH_i to a more alkaline value while, at the same time, acidifying the lumen. We believe that this phase likely represents the activity of the apical V-ATPase, and our data demonstrate that acidification of the lumen below pH ~5.5 requires VHA-6.

Finally, calcium oscillations are thought to drive pH fluctuations during defecation. Although we did not expect to find a role for VHA-6 in calcium signaling, as a control we employed the genetic indicator cameleon YC6.1 to measure calcium. As predicted, *vha-6* RNAi-treated worms, similar to wild-type worms, exhibited robust oscillations during defecation (e.g., see the first 300 s of the trace in supplemental Fig. S3).

Despite reductions in the magnitude of cellular and luminal pH oscillations, measurements of pBoc strength indicated that the posterior body wall muscles were contracting normally during defecation (Table 1). The pBoc contraction is caused by ligand binding of protons to a body wall muscle receptor protein, PBO-5 (3), and a normal contraction strength suggests normal proton extrusion across the basolateral membrane. To measure extracellular pH of the pseudocoelom between the intestine and body wall muscle, we used a posterior intestinal cell-specific promoter fusion of pHluorin to a partial PAT-3 integrin cDNA (51). In control and *vha-6(RNAi)* worms, robust extracellular pH oscillations occurred coincident with pBoc (Fig. 3*C*). The average values were nearly identical, with a resting pH ~7.35 and nadir pH ~6.5 (see supplemental Figs. S1E and S1F). The duration of the acidic pulse (pH <6.8) was ~5 s, which is similar to the duration of the posterior body wall muscle contraction during defecation. This normal pBoc likely reflects the combination of normal calcium signaling and intracellular acidification that occurs in the *vha-6(RNAi)* worms (i.e., the nadir pH in Fig. 3*A* is nearly identical in both traces).

Finally, the pH of the lumen in *vha-6(RNAi)* worms was noted to be slightly acidic, despite an apparent lack of proton pumping, and we hypothesized that this was due to equilibration with the growth medium, which was buffered to pH ~5.6. Attempts to grow the worms on plates buffered at a higher pH quickly inhibited intestinal calcium oscillations (see supplemental Fig. S3A), which are the driving force for defecation and occur upstream of pH oscillations (see supplemental Fig. S3B); thus we cannot comment directly on how luminal alkalinization above pH 6 affects defecation. However, it is intriguing that placement of wild-type worms, which can survive at pH extremes from 3 to ~11 (33), onto high-pH plates has very little effect on luminal pH, pH oscillations, or defecation behavior (E. Allman, unpublished data). These strong protective mechanisms suggest the importance of luminal pH for normal and adaptive physiology.

Deficit in VHA-6 activity reduces intestinal nutrient uptake and fat accumulation. We recently theorized that the movement of protons into the cell during defecation may help preserve them during expulsion of the luminal contents (51). This would make sense if the proton gradient was crucial for absorbing required nutrients into the intestine and fits well with the larva arrest phenotype observed in the *vha-6* mutant. There is precedence for operation of proton-coupled nutrient uptake pathways in worms, such as the proton-dipeptide symporter OPT-2 (42, 44). Therefore, we assessed the consequences of disrupting *vha-6* expression on fat content and nutrient uptake. Because larva exhibit a reduced fat mass compared with adults, we initiated RNAi at the L2 stage, which allowed more of the *vha-6*-deficient worms to mature to early adulthood for comparison with the adult control worms.

Worms lack dedicated adipose tissue and, instead, store fat primarily in the intestinal epithelial cells; lipid droplets have been observed in the hypodermis as well (2, 34). Oil Red O staining in fixed samples confirmed a reduction of whole body fat mass in young adult *vha-6(RNAi)* worms compared with control worms (Fig. 4). This is consistent with the reduced growth rate, decreased body size, and small brood size associated with the loss of the V-ATPase a-subunit. Interestingly, the staining of mature oocytes near the spermatheca, where fertilization occurs, was not compromised (arrows in Fig. 4*B*). We also found that the lumens of the *vha-6(RNAi)* worms occasionally appeared swollen, with a concomitant reduction of the cytoplasmic contents of the intestinal cells; this phenotype was variably penetrant and might relate to a lack of substrates reducing the size of this fat storage tissue or electrolyte imbalance.

Given the lack of fat stores and slow growth phenotype, we predicted that the worms were not getting enough nutrients. The uptake of nutrients in the mammalian intestine is known to be influenced by V-ATPase activity, and proton-coupled nutrient uptake is thought to be important in worms as well. Absorption of dipeptides in the nematode intestine is com-

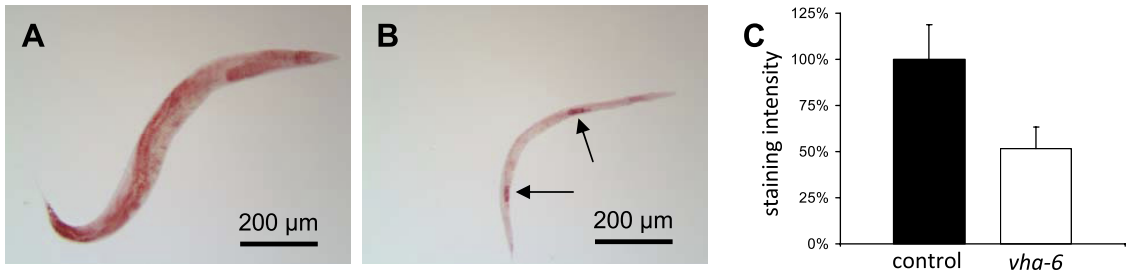

Fig. 4. Analysis of fat storage. Images of Oil Red O-stained lipid droplets suggest a severe reduction of fat mass in small, adult *vha-6(RNAi)* worms (*B*) compared with adult control worms (*A*). Quantification of staining intensity (*C*) confirmed a large reduction of whole body fat mass after *vha-6* targeting ($n = 20$, $P < 0.01$); background staining was negligible. Arrows in *B* denote mature oocytes, which retain Oil Red O staining, even in the absence of VHA-6, and contribute to the total body fat mass shown in *C*.

pletely dependent on the proton-dipeptide symporter OPT-2 (17, 42), which is a functional ortholog of mammalian PepT1; PepT1 and OPT-2 activity have been linked to regulators of pH such as sodium-proton exchangers (32, 44, 65, 66), and presumably dipeptide transport would be accelerated by a sharp proton gradient, such as that created by V-ATPase pumping protons into the lumen.

To test this idea, we examined the absorption of the fluorescent AMCA-labeled dipeptide Ala-Lys (kindly provided by Dr. H. Daniel), which has been used as a model substrate to study dipeptide uptake in mammals (20, 21) and worms (42). The intestinal dipeptide pool in control worms appeared to reside in discrete intracellular storage organelles, and a severe reduction of signal followed the loss of *vha-6* expression (Fig. 5, also see supplemental Fig. S2). This was due mainly to a decrease in the number of granules and less to a decrease in the staining intensity of individual granules (see supplemental Fig. S2). The reduced uptake was not due solely to the biological age of the worms, inasmuch as L3 stage control worms stained nearly as well as adults (see supplemental Fig. S2). These results suggest that the accumulation of intestinal dipeptide stores requires VHA-6, perhaps through physiologically coupled uptake mechanisms. However, even though the VHA-6::mCherry fusion protein does not localize to intracellular organelles (Fig. 1*D*), we cannot definitively rule out a role for VHA-6 in the biogenesis of the storage granules themselves.

In fact, the formation of acidic lysosomes has been shown to require V-ATPase activity in worms (48), and fat storage granules are specialized lysosome-related organelles (14, 24, 53, 55). Given the lack of fat storage granules in the intestine of *vha-6* mutants, we used LysoTracker Red to determine whether disruption of *vha-6* expression altered staining of acidic organelles in RNAi-treated worms (Fig. 6, *A–D*). Briefly, we found no change in the appearance or density of LysoTracker Red-positive organelles between *vha-6*(RNAi) and control worms, even when comparing the slowest growing (and presumably most depleted of VHA-6) worms (Fig. 6*C*) with the L4 stage/young adult population of control worms (Fig. 6*A*). Similar results were obtained using acridine orange labeling (data not shown). Since one could argue that the acidic compartments we labeled were formed during embryogenesis, before the worms were subjected to RNAi, and persisted into adulthood, despite RNAi, we used a complementary approach that involved the *vha-6(ok1825)* deletion mutant (Fig. 6, *E* and *F*). Autofluorescent material that is present in the embryonic intestine is thought to reflect newly synthesized acidified lysosomes that are destined to store fat (24). We examined autofluorescent emissions in mosaic animals from the *vha-6* transgenic rescue line and found nearly identical patterns of embryonic intestinal autofluorescence in rescued and nonrescued siblings (Fig. 6, *E* and *F*). These results confirm that VHA-6 acts at the apical membrane, rather than contributing to the acidification of intracellular organelles.

DISCUSSION

The twin discoveries of the H^+-K^+-ATPase of gastric parietal cells as the pump involved in proton secretion into the gastric lumen (18) and *Helicobacter pylori* infection as the main cause of gastric and duodenal ulcers (41) provided a mechanism and a target for treating acid-peptic disorders. Despite the effectiveness of PPIs as a therapeutic tool, there remain significant gaps in our knowledge of how H^+-K^+-ATPase regulation occurs, as well as how H^+-K^+-ATPases regulate other processes in the cell. For example, proton secretion can be controlled by recycling of V-ATPase-contain-

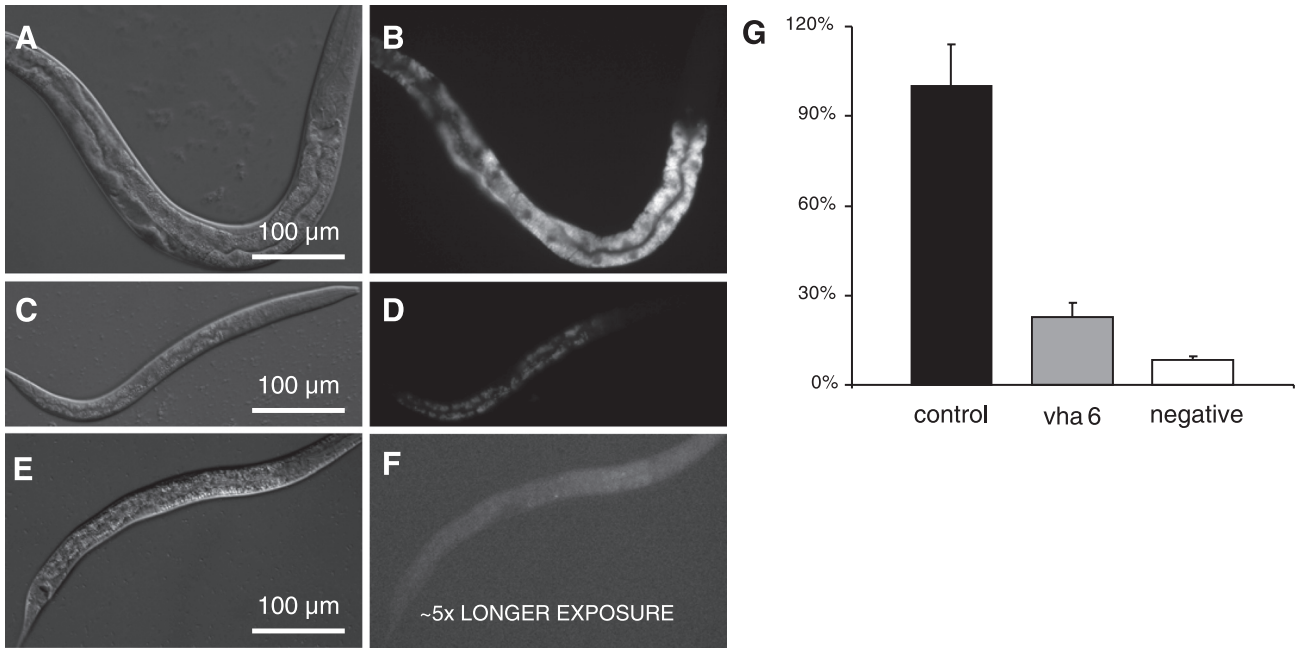

Fig. 5. Analysis of nutrient uptake. DIC (*A, C*, and *E*) and corresponding fluorescent (*B, D*, and *F*) images of control (*A* and *B*) and *vha-6(RNAi)* (*C* and *D*) worms that were, after 48 h of RNAi, cultured overnight in liquid medium containing a bacterial food source and AMCA-labeled Ala-Lys dipeptide. Negative controls (wild-type larva, no dipeptide; *E* and *F*) displayed slight fluorescence, despite longer exposure. Quantification of staining intensity (*G*) confirms a significant reduction of dipeptide uptake ($n = 10$, $P < 0.01$).

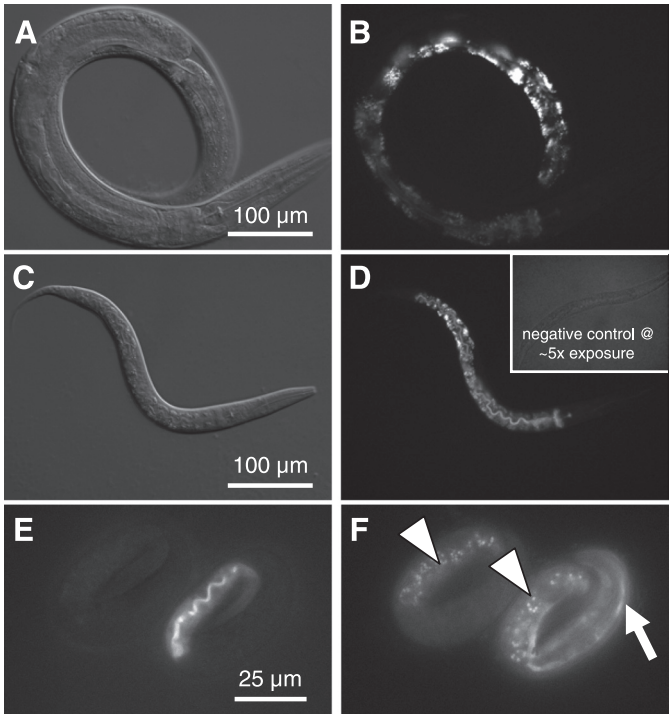

Fig. 6. Analysis of acidic gut granules in adult worms. LysoTracker Red was used to stain acidic gut granules in 3-day-old control (*A* and *B*) and *vha-6(RNAi)* worms (*C* and *D*). Staining intensity varied along the length of the intestine, with posterior intestinal cells displaying the brightest signal. Control and *vha-6(RNAi)* worms stained similarly, despite the obvious difference in developmental age (L2 vs. young adult); developmentally matched worms similarly showed no obvious differences in the formation of acidic granules. *Inset* in *D* shows a negative control (without LysoTracker Red) that was exposed 5 times as long, demonstrating lack of background. For examination of autofluorescent gut granules, 3-fold embryos from the mosaic *vha-6(ok1825)* P*vha-6*::VHA-6::mCherry rescue line were imaged at 555-nm excitation and 590-nm emission for transgene expression (*E*) and at 340-nm excitation and 535-nm emission for autofluorescence (*F*). Embryo at *right* is expressing mCherry rescue marker at the apical membrane of the lumen, which fluoresces red (*E*), as well as a muscle P*myo-3*::GFP marker used to track the transgene (arrow in *F*). Embryo at *left* lacks both transgenes, yet it accumulates UV-excitable autofluorescent gut granules (arrowheads in *F*) to the same extent as its transgenic sibling, indicating that successful biogenesis of these acidic intracellular storage compartments occurs in the complete absence of *vha-6* expression.

ing vesicles to and from the plasma membrane (1, 9), whereas subunit assembly of organelle-associated V-ATPases has been shown to be modulated by the reversible assembly of V_1 and V_0 complexes into the holoenzyme in the *Mandusa sexta* larval midgut (60), yeast (for review see Ref. 47), and, more recently, mammalian renal epithelial cells (54). Nonetheless, the mechanisms that regulate these processes are not fully understood. Furthermore, there is some evidence that V-ATPases might act as proton sensors that enable the recruitment of cytosolic proteins and their trafficking through endosomal degradative pathways (26).

In the present study, we have established *C. elegans* as a simple genetic model for studying H^+-K^+-ATPase-mediated acid secretion into the lumen of the gut. Our observation that the nematode intestinal H^+-K^+-ATPase a-subunit VHA-6 is essential for establishing ion gradients that form the basis of the rhythmic defecation cycle sets up a powerful system for studying regulation of its transport activity. The DMP is executed at ~45-s intervals and is timed by oscillatory calcium signaling in the intestine (15). We have previously shown that calcium oscillations trigger an influx of protons from the intestinal lumen (51). In response, proton extrusion occurs across the basolateral membrane, and protons are the ligand for a muscle receptor that mediates contractions (3). However, as we have demonstrated in the present study, reacidification of the lumen to normal resting values requires the activity of VHA-6. Since pumping protons out of the cell requires ATP, this process must be carefully regulated to prevent wasting energy. Therefore, it is interesting that, despite robust cellular acidification, protons do not appear to be pumped into the lumen until calcium has returned to baseline levels, suggesting some level of communication between calcium and pH as signaling molecules. It is intriguing that regulation of V-ATPase activity through subunit assembly has been shown to involve calcium signaling in yeast and humans (6, 54). Given that defecation is initiated through oscillatory calcium signaling, it is possible that the worm V-ATPase complex could serve as a model for studying rhythmic subunit assembly and/or trafficking.

Insect epithelia have historically provided a robust model for active transepithelial cation transport, with Malphighian tubules and larval gut segments being the focus of numerous studies in *Aedes aegypti* as well as the genetic model *Drosophila melanogaster* (for review see Ref. 71). From these studies, a variety of models have emerged showing that V-ATPase activity energizes secondary active transport processes that are specific to the tissue in question and allow cations, bicarbonate, and/or nutrients to move across apical and basolateral membranes. Although V-ATPases can be the primary energizer of epithelial cell secretion and absorption, in general, these processes are homeostatic, creating lasting gradients that facilitate cell function, although they likely respond to environmental influences, such as nutrient or solute availability, as well. One advantage to studying V-ATPase activity as pertains to the nematode defecation cycle is that we are able to observe its effects at ~45-s intervals in the form of intestinal pH oscillations. Although these pH oscillations appear to be the primary physiological output of the apical V-ATPase, as is the case with insects, it is likely that multiple secondary active transport processes are coupled to the formation of the proton gradient. For example, it is well established that acid facilitates the digestion of protein and the absorption of iron, calcium, and vitamin B12 in mammals.

This may also be true in nematodes, inasmuch as v*ha-6* is necessary for the proper development of *C. elegans* past the L1 stage. In support of this idea, RNAi phenocopies the *vha-6* deletion mutant and causes an L1 arrest, whereas single-generation treatment starting as L1 larva results in slow growth and, eventually, stalled development (Fig. 2). Moreover, in the older, stalled worms, dramatic effects are observed on fat accumulation and dipeptide uptake, which occurs through the proton-dipeptide symporter OPT-2 (42). A recent report has defined a class of intestinal granules where transporter associated with antigen processing-like (TAPL) ABC transporters likely facilitate peptide uptake into nonacidic, but lysosome-associated membrane protein-positive, intestinal organelles presumably related to lysosomes (31). Colabeling will be necessary to define whether these organelles are the same as the AMCA-labeled granules we observe in the present study,

but it is unlikely that dipeptides are the only nutrient whose uptake is affected by the loss of *vha-6*. For example, V-ATPase activity in *Ae. aegypti* is coupled electrogenically to Na-amino acid transport (22), and pH homeostasis has recently been shown to be important for the uptake of free fatty acids from the nematode lumen (59).

Despite the apparent link between luminal pH and nutrient uptake, growing worms at pH 4 does not rescue the *vha-6* mutant phenotype and, in fact, causes cellular acidosis (E. Allman and K. Nehrke, unpublished observations). It is reasonable to assume that the lack of an apical V-ATPase results in an inability to clear protons arising from catabolic processes in the cell, consistent with a role for V-ATPase in maintaining intra- and extracellular pH homeostasis.

If the proton gradient created across the intestinal apical membrane by VHA-6 does drive nutrient absorption, consistent with the role of the gastric H^+-K^+-ATPase in mammals, then a partial reduction of the proton gradient (such as occurs via RNAi) should result in caloric restriction (or a partial starvation). In support of this idea, postdevelopmental RNAi targeting of *vha-6* expression in adults leads to an increase in mean lifespan from 17 days in control worms to 20 days in the

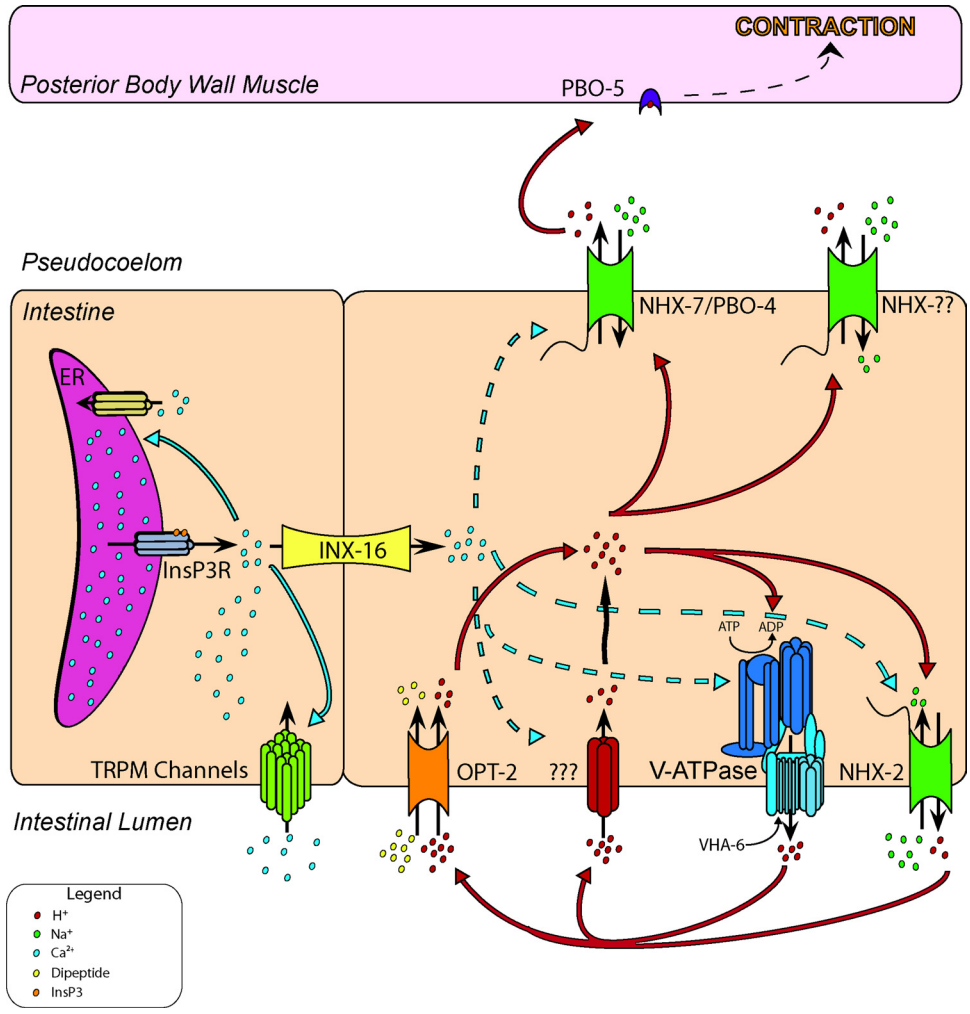

Fig. 7. Schematic of rhythmic intestinal electrolyte transport during defecation in worms. Resting pH of the intestinal cell and the pseudocoelomic fluid that bathes the cell's basolateral surface is near a physiological norm of 7.4. Lumen of the intestine is acidic, with pH closer to 4. Cell-autonomous oscillatory calcium signaling involving activation of inositol 1,4,5-trisphosphate receptor ($InsP_3R$) underlies the defecation pacemaker and triggers calcium inflow through the transient receptor potential melastatin channels GTL-1 and GON-2. A calcium wave propagates through the intestine, moving between adjacent intestinal cells through the gap junction protein INX-16. Elevations in calcium appear to cause the apical membrane to become permeable to protons, which enter the cell through an unknown mechanism. As protons flow down the transmembrane gradient, the cell acidifies and the lumen alkalinizes. In response to acidification and, perhaps, calcium as well, the Na^+/H^+ exchanger PBO-4/NHX-7 extrudes protons across the basolateral membrane. Protons trigger the first muscle contraction (pBoc) in the defecation motor program by binding to the muscle cell receptor PBO-5. Calcium returns to baseline levels in part through the activity of SCA-1 (SERCA), the endoplasmic reticular (ER) membrane ATPase, and pH_i gradually recovers from acidification. This process likely involves Na^+-H^+ antiport and V-ATPase activities (see Fig. 3) but does not require NHX-7, which acts in a signaling, rather than a homeostatic, pathway. Eventually, luminal pH reaches ~4, at which point the cytoplasm begins to acidify slightly. We hypothesize that this occurs as a result of metabolic processes that result in proton accumulation in the cell and inability of VHA-6 to export these protons, because the pH gradient has become too steep or because of some unknown regulatory pathway involving perhaps trafficking or subunit disassembly. In most acid-secreting mammalian systems, proton pumping requires the activity of apical K^+ and Cl^- channels (such as KCNE2 and CFTR); whether this holds true in worms as well is under investigation. Finally, protons that have been pumped into the lumen work to allow nutrient absorption though proton-coupled uptake pathways such as the H^+-dipeptide symporter OPT-2. This is a representative, rather than an exhaustive, depiction of the transporters that function in defecation.

vha-6(RNAi) worms (see supplemental Fig. S4). Although VHA-6 certainly plays a role in facilitating proton pumping activity by the apical V-ATPase, we acknowledge that VHA-6 may also recruit cytosolic proteins to the membrane and that the lack of these proteins could have an indirect effect on nutrient absorption or fat metabolism. However, any activity of VHA-6 not related to proton pumping would be expected to occur at the apical membrane because of its restricted expression there, and we have shown that VHA-6 does not contribute to the acidification of terminally mature lysosomes, as the gut storage granules have been suggested to be (24, 53, 55). Nonetheless, the absence of intestinal Oil Red O staining suggests a loss of fat mass, perhaps downstream of a deficit in nutrient uptake.

So why couple nutrient uptake and defecation through pH? One reason may have to do with the ability to modulate behavior based on environmental conditions. *C. elegans* cease defecation in the absence of food (40), and extensions in cycle period are common under conditions of caloric restriction. Nutrient deprivation would be expected to reduce energy production, which would lead to a reduction of V-ATPase activity. We have shown that the loss of V-ATPase activity extends the defecation period, and this should allow more time for nutrient uptake. Whether this is a function of luminal or cytoplasmic pH homeostasis, however, is unknown.

We are just starting to understand the functional interactions between nutrient uptake, energy production, pH regulation, and oscillatory calcium signaling during defecation, and the data that we have presented establishes a basis for future integrative studies of H^+-K^+-ATPase activity in intestinal function, ion transport, and metabolism in this genetic model organism. Figure 7 is a schematic of ion transport processes highlighting calcium and proton movement during defecation and the membrane transporters that are involved, as well as potential relationships between these transporters. Future studies will undoubtedly fill in some of the blanks, such as the molecular identity of the proton influx pathway at the apical membrane and definition of mechanisms for cross talk between pH and calcium signaling.

ACKNOWLEDGMENTS

We thank Teresa Sherman for expert technical assistance.

GRANTS

This work was supported in part by National Heart, Lung, and Blood Institute Grant R01 HL-080810 and National Science Foundation Grant IOS-0919848 (K. Nehrke). D. Johnson was supported by National Institute of General Medical Sciences Grant F31 GM-084506.

REFERENCES

1. **Al-Awqati Q.** Plasticity in epithelial polarity of renal intercalated cells: targeting of the H^+-ATPase and band 3. *Am J Physiol Cell Physiol* 270: C1571–C1580, 1996.
2. **Ashrafi K, Chang FY, Watts JL, Fraser AG, Kamath RS, Ahringer J, Ruvkun G.** Genome-wide RNAi analysis of *Caenorhabditis elegans* fat regulatory genes. *Nature* 421: 268–272, 2003.
3. **Beg AA, Ernstrom GG, Nix P, Davis MW, Jorgensen EM.** Protons act as a transmitter for muscle contraction in *C. elegans*. *Cell*: 149–160, 2008.
4. **Beyenbach KW, Wieczorek H.** The V-type H^+ ATPase: molecular structure and function, physiological roles and regulation. *J Exp Biol* 209: 577–589, 2006.
5. **Blair HC, Teitelbaum SL, Ghiselli R, Gluck S.** Osteoclastic bone resorption by a polarized vacuolar proton pump. *Science* 245: 855–857, 1989.
6. **Brandao RL, de Magalhaes-Rocha NM, Alijo R, Ramos J, Thevelein JM.** Possible involvement of a phosphatidylinositol-type signaling pathway in glucose-induced activation of plasma membrane H^+-ATPase and cellular proton extrusion in the yeast *Saccharomyces cerevisiae*. *Biochim Biophys Acta* 1223: 117–124, 1994.
7. **Brenner S.** The genetics of *Caenorhabditis elegans*. *Genetics* 77: 71–94, 1974.
8. **Breton S, Brown D.** New insights into the regulation of V-ATPase-dependent proton secretion. *Am J Physiol Renal Physiol* 292: F1–F10, 2007.
9. **Brown D, Breton S.** H^+-V-ATPase-dependent luminal acidification in the kidney collecting duct and the epididymis/vas deferens: vesicle recycling and transcytotic pathways. *J Exp Biol* 203: 137–145, 2000.
10. **Brown D, Breton S.** Mitochondria-rich, proton-secreting epithelial cells. *J Exp Biol* 199: 2345–2358, 1996.
11. **Brown D, Hirsch S, Gluck S.** Localization of a proton-pumping ATPase in rat kidney. *J Clin Invest* 82: 2114–2126, 1988.
12. **Croll NA, Smith JM.** Integrated behavior in the feeding phase of *Caenorhabditis elegans* (Nematoda). *J Zool* 184: 507–517, 1978.
13. **Curran SP, Ruvkun G.** Lifespan regulation by evolutionarily conserved genes essential for viability. *PLoS Genet* 3: e56, 2007.
14. **Currie E, King B, Lawrenson AL, Schroeder LK, Kershner AM, Hermann GJ.** Role of the *Caenorhabditis elegans* multidrug resistance gene, *mrp-4*, in gut granule differentiation. *Genetics* 177: 1569–1582, 2007.
15. **Dal Santo P, Logan MA, Chisholm AD, Jorgensen EM.** The inositol trisphosphate receptor regulates a 50-second behavioral rhythm in *C. elegans*. *Cell* 98: 757–767, 1999.
16. **Espelt MV, Estevez AY, Yin X, Strange K.** Oscillatory Ca^{2+} signaling in the isolated *Caenorhabditis elegans* intestine: role of the inositol-1,4,5-trisphosphate receptor and phospholipases Cβ and -γ. *J Gen Physiol* 126: 379–392, 2005.
17. **Fei YJ, Fujita T, Lapp DF, Ganapathy V, Leibach FH.** Two oligopeptide transporters from *Caenorhabditis elegans*: molecular cloning and functional expression. *Biochem J* 332: 565–572, 1998.
18. **Fellenius E, Berglindh T, Sachs G, Olbe L, Elander B, Sjostrand SE, Wallmark B.** Substituted benzimidazoles inhibit gastric-acid secretion by blocking (H^+-K^+)ATPase. *Nature* 290: 159–161, 1981.
19. **Forgac M.** Vacuolar ATPases: rotary proton pumps in physiology and pathophysiology. *Nat Rev Mol Cell Biol* 8: 917–929, 2007.
20. **Groneberg DA, Döring F, Eynott PR, Fischer A, Daniel H.** Intestinal peptide transport: ex vivo uptake studies and localization of peptide carrier PEPT1. *Am J Physiol Gastrointest Liver Physiol* 281: G697–G704, 2001.
21. **Groneberg DA, Eynott PR, Döring F, Thai Dinh Q, Oates T, Barnes PJ, Chung KF, Daniel H, Fischer A.** Distribution and function of the peptide transporter PEPT2 in normal and cystic fibrosis human lung. *Thorax* 57: 55–60, 2002.
22. **Harvey WR, Boudko DY, Rheault MR, Okech BA.** NHEVNAT: an H^+ V-ATPase electrically coupled to a Na^+:nutrient amino acid transporter (NAT) forms an Na^+/H^+ exchanger (NHE). *J Exp Biol* 212: 347–357, 2009.
23. **Havu N.** Enterochromaffin-like cell carcinoids of gastric mucosa in rats after life-long inhibition of gastric secretion. *Digestion* 35 *Suppl* 1: 42–55, 1986.
24. **Hermann GJ, Schroeder LK, Hieb CA, Kershner AM, Rabbitts BM, Fonarev P, Grant BD, Priess JR.** Genetic analysis of lysosomal trafficking in *Caenorhabditis elegans*. *Mol Biol Cell* 16: 3273–3288, 2005.
25. **Hinton A, Bond S, Forgac M.** V-ATPase functions in normal and disease processes. *Pflügers Arch* 457: 589–598, 2009.
26. **Hurtado-Lorenzo A, Skinner M, El Annan J, Futai M, Sun-Wada GH, Bourgoin S, Casanova J, Wildeman A, Bechoua S, Ausiello DA, Brown D, Marshansky V.** V-ATPase interacts with ARNO and Arf6 in early endosomes and regulates the protein degradative pathway. *Nat Cell Biol* 8: 124–136, 2006.
27. **Iwasaki K, Liu DW, Thomas JH.** Genes that control a temperature-compensated ultradian clock in *Caenorhabditis elegans*. *Proc Natl Acad Sci USA* 92: 10317–10321, 1995.
28. **Josephsen K, Praetorius J, Frische S, Gawenis LR, Kwon TH, Agre P, Nielsen S, Fejerskov O.** Targeted disruption of the Cl^-/HCO_3^- exchanger Ae2 results in osteopetrosis in mice. *Proc Natl Acad Sci USA* 106: 1638–1641, 2009.
29. **Kamath RS, Fraser AG, Dong Y, Poulin G, Durbin R, Gotta M, Kanapin A, Le Bot N, Moreno S, Sohrmann M, Welchman DP,**

Zipperlen P, Ahringer J. Systematic functional analysis of the *Caenorhabditis elegans* genome using RNAi. *Nature* 421: 231–237, 2003.
30. **Karet FE, Finberg KE, Nelson RD, Nayir A, Mocan H, Sanjad SA, Rodriguez-Soriano J, Santos F, Cremers CW, Di Pietro A, Hoffbrand BI, Winiarski J, Bakkaloglu A, Ozen S, Dusunsel R, Goodyer P, Hulton SA, Wu DK, Skvorak AB, Morton CC, Cunningham MJ, Jha V, Lifton RP.** Mutations in the gene encoding β_1 subunit of H^+-ATPase cause renal tubular acidosis with sensorineural deafness. *Nat Genet* 21: 84–90, 1999.
31. **Kawai H, Tanji T, Shiraishi H, Yamada M, Iijima R, Inoue T, Kezuka Y, Ohashi K, Yoshida Y, Tohyama K, Gengyo-Ando K, Mitani S, Arai H, Ohashi-Kobayashi A, Maeda M.** Normal formation of a subset of intestinal granules in *Caenorhabditis elegans* requires ABC transporters HAF-4 and HAF-9, which are highly homologous to human lysosomal peptide transporter TAPL (TAP-like). *Mol Biol Cell* 20: 2979–2990, 2009.
32. **Kennedy DJ, Leibach FH, Ganapathy V, Thwaites DT.** Optimal absorptive transport of the dipeptide glycylsarcosine is dependent on functional Na^+/H^+ exchange activity. *Pflügers Arch* 445: 139–146, 2002.
33. **Khanna N, Cressman CP, Tatara CP, Williams PL.** Tolerance of the nematode *Caenorhabditis elegans* to pH, salinity, and hardness in aquatic media. *Arch Environ Contam Toxicol* 32: 110–114, 1997.
34. **Kimura KD, Tissenbaum HA, Liu Y, Ruvkun G.** *daf-2*, an insulin receptor-like gene that regulates longevity and diapause in *Caenorhabditis elegans*. *Science* 277: 942–946, 1997.
35. **Kontani K, Moskowitz IP, Rothman JH.** Repression of cell-cell fusion by components of the *C. elegans* vacuolar ATPase complex. *Dev Cell* 8: 787–794, 2005.
36. **Kornak U, Kasper D, Bosl MR, Kaiser E, Schweizer M, Schulz A, Friedrich W, Delling G, Jentsch TJ.** Loss of the ClC-7 chloride channel leads to osteopetrosis in mice and man. *Cell* 104: 205–215, 2001.
37. **Kornak U, Schulz A, Friedrich W, Uhlhaas S, Kremens B, Voit T, Hasan C, Bode U, Jentsch TJ, Kubisch C.** Mutations in the a3 subunit of the vacuolar H^+-ATPase cause infantile malignant osteopetrosis. *Hum Mol Genet* 9: 2059–2063, 2000.
38. **Lamberts R, Brunner G, Solcia E.** Effects of very long (up to 10 years) proton pump blockade on human gastric mucosa. *Digestion* 64: 205–213, 2001.
39. **Liegeois S, Benedetto A, Garnier JM, Schwab Y, Labouesse M.** The V_0-ATPase mediates apical secretion of exosomes containing hedgehog-related proteins in *Caenorhabditis elegans*. *J Cell Biol* 173: 949–961, 2006.
40. **Liu DW, Thomas JH.** Regulation of a periodic motor program in *C. elegans*. *J Neurosci* 14: 1953–1962, 1994.
41. **Marshall BJ, Warren JR.** Unidentified curved bacilli in the stomach of patients with gastritis and peptic-ulceration. *Lancet* 1: 1311–1315, 1984.
42. **Meissner B, Boll M, Daniel H, Baumeister R.** Deletion of the intestinal peptide transporter affects insulin and TOR signaling in *Caenorhabditis elegans*. *J Biol Chem* 279: 36739–36745, 2004.
43. **Miesenbock G, De Angelis DA, Rothman JE.** Visualizing secretion and synaptic transmission with pH-sensitive green fluorescent proteins. *Nature* 394: 192–195, 1998.
44. **Nehrke K.** A reduction in intestinal cell pH_i due to loss of the *Caenorhabditis elegans* Na^+/H^+ exchanger NHX-2 increases life span. *J Biol Chem* 278: 44657–44666, 2003.
45. **Nehrke K, Denton J, Mowrey W.** Intestinal Ca^{2+} wave dynamics in freely moving *C. elegans* coordinate execution of a rhythmic motor program. *Am J Physiol Cell Physiol* 294: C333–C344, 2008.
46. **Neutzsky-Wulff AV, Karsdal MA, Henriksen K.** Characterization of the bone phenotype in ClC-7-deficient mice. *Calcif Tissue Int* 83: 425–437, 2008.
47. **Nishi T, Forgac M.** The vacuolar H^+-ATPases—nature's most versatile proton pumps. *Nat Rev Mol Cell Biol* 3: 94–103, 2002.
48. **Oka T, Futai M.** Requirement of V-ATPase for ovulation and embryogenesis in *Caenorhabditis elegans*. *J Biol Chem* 275: 29556–29561, 2000.
49. **Oka T, Toyomura T, Honjo K, Wada Y, Futai M.** Four subunit a isoforms of *Caenorhabditis elegans* vacuolar H^+-ATPase. Cell-specific expression during development. *J Biol Chem* 276: 33079–33085, 2001.
50. **Peters MA, Teramoto T, White JQ, Iwasaki K, Jorgensen EM.** A calcium wave mediated by gap junctions coordinates a rhythmic behavior in *C. elegans*. *Curr Biol* 17: 1601–1608, 2007.
51. **Pfeiffer J, Johnson D, Nehrke K.** Oscillatory transepithelial H^+ flux regulates a rhythmic behavior in *C. elegans*. *Curr Biol* 18: 297–302, 2008.
52. **Pujol N, Bonnerot C, Ewbank JJ, Kohara Y, Thierry-Mieg D.** The *Caenorhabditis elegans unc-32* gene encodes alternative forms of a vacuolar ATPase a subunit. *J Biol Chem* 276: 11913–11921, 2001.
53. **Rabbitts BM, Ciotti MK, Miller NE, Kramer M, Lawrenson AL, Levitte S, Kremer S, Kwan E, Weis AM, Hermann GJ.** *glo-3*, a novel *Caenorhabditis elegans* gene, is required for lysosome-related organelle biogenesis. *Genetics* 180: 857–871, 2008.
54. **Sautin YY, Lu M, Gaugler A, Zhang L, Gluck SL.** Phosphatidylinositol 3-kinase-mediated effects of glucose on vacuolar H^+-ATPase assembly, translocation, and acidification of intracellular compartments in renal epithelial cells. *Mol Cell Biol* 25: 575–589, 2005.
55. **Schroeder LK, Kremer S, Kramer MJ, Currie E, Kwan E, Watts JL, Lawrenson AL, Hermann GJ.** Function of the *Caenorhabditis elegans* ABC transporter PGP-2 in the biogenesis of a lysosome-related fat storage organelle. *Mol Biol Cell* 18: 995–1008, 2007.
56. **Schubert ML, Peura DA.** Control of gastric acid secretion in health and disease. *Gastroenterology* 134: 1842–1860, 2008.
57. **Siklos S, Jasper J, Wicks S, Rankin C.** Interactions between an endogenous oscillator and response to TAP in *C. elegans*. *Psychobiology* 28: 571–580, 2000.
58. **Sly WS, Hewett-Emmett D, Whyte MP, Yu YS, Tashian RE.** Carbonic anhydrase II deficiency identified as the primary defect in the autosomal recessive syndrome of osteopetrosis with renal tubular acidosis and cerebral calcification. *Proc Natl Acad Sci USA* 80: 2752–2756, 1983.
59. **Spanier B, Lasch K, Marsch S, Benner J, Liao W, Hu H, Kienberger H, Eisenreich W, Daniel H.** How the intestinal peptide transporter PEPT-1 contributes to an obesity phenotype in *Caenorhabditis elegans*. *PLoS ONE* 4: e6279, 2009.
60. **Sumner JP, Dow JAT, Earley FGP, Klein U, Jäger D, Wieczorek H.** Regulation of plasma membrane V-ATPase activity by dissociation of peripheral subunits. *J Biol Chem* 270: 5649–5653, 1995.
61. **Syntichaki P, Samara C, Tavernarakis N.** The vacuolar H^+-ATPase mediates intracellular acidification required for neurodegeneration in *C. elegans*. *Curr Biol* 15: 1249–1254, 2005.
62. **Teramoto T, Iwasaki K.** Intestinal calcium waves coordinate a behavioral motor program in *C. elegans*. *Cell Calcium* 40: 319–327, 2006.
63. **Thomas JA, Buchsbaum RN, Zimniak A, Racker E.** Intracellular pH measurements in Ehrlich ascites tumor cells utilizing spectroscopic probes generated in situ. *Biochemistry* 18: 2210–2218, 1979.
64. **Thomas JH.** Genetic analysis of defecation in *Caenorhabditis elegans*. *Genetics* 124: 855–872, 1990.
65. **Thwaites DT, Ford D, Glanville M, Simmons NL.** H^+/solute-induced intracellular acidification leads to selective activation of apical Na^+/H^+ exchange in human intestinal epithelial cells. *J Clin Invest* 104: 629–635, 1999.
66. **Thwaites DT, Kennedy DJ, Raldua D, Anderson CM, Mendoza ME, Bladen CL, Simmons NL.** H/dipeptide absorption across the human intestinal epithelium is controlled indirectly via a functional Na/H exchanger. *Gastroenterology* 122: 1322–1333, 2002.
67. **Toyomura T, Murata Y, Yamamoto A, Oka T, Sun-Wada GH, Wada Y, Futai M.** From lysosomes to the plasma membrane: localization of vacuolar-type H^+-ATPase with the a_3 isoform during osteoclast differentiation. *J Biol Chem* 278: 22023–22030, 2003.
68. **Toyomura T, Oka T, Yamaguchi C, Wada Y, Futai M.** Three subunit a isoforms of mouse vacuolar H^+-ATPase. Preferential expression of the a_3 isoform during osteoclast differentiation. *J Biol Chem* 275: 8760–8765, 2000.
69. **Truong K, Sawano A, Mizuno H, Hama H, Tong KI, Mal TK, Miyawaki A, Ikura M.** FRET-based in vivo Ca^{2+} imaging by a new calmodulin-GFP fusion molecule. *Nat Struct Biol* 8: 1069–1073, 2001.
70. **Venta PJ, Shows TB, Curtis PJ, Tashian RE.** Polymorphic gene for human carbonic anhydrase II: a molecular disease marker located on chromosome 8. *Proc Natl Acad Sci USA* 80: 4437–4440, 1983.
71. **Wieczorek H, Beyenbach KW, Huss M, Vitavska O.** Vacuolar-type proton pumps in insect epithelia. *J Exp Biol* 212: 1611–1619, 2009.
72. **Xu J, Cheng T, Feng HT, Pavlos NJ, Zheng MH.** Structure and function of V-ATPases in osteoclasts: potential therapeutic targets for the treatment of osteolysis. *Histol Histopathol* 22: 443–454, 2007.